Indian Conference on
GEOTECHNICAL AND GEO-ENVIRONMENTAL ENGINEERING (ICGGE-2019)
March 01-02, 2019
MNNIT Allahabad, Prayagraj, India.

FINDING LIQUEFACTION FEATURES BY USING SATELLITE DATA FOR NORTH-EAST INDIA REGION

Niranjan Borah
Deptt. of Civil Engineering, Indian Institute of Technology Guwahati, Assam, India
Email: niran521152@gmail.com

Abhishek Kumar
Deptt. of Civil Engineering, Indian Institute of Technology Guwahati, Assam, India
Email: abhiak@iitg.ac.in

ABSTRACT: Pre and post-earthquake(EQ) satellite images of area near the source of the 2016 Manipur EQ are used for finding the probable liquefaction. Liquefaction-induced surface effects are identified by measuring the increase in moisture content of the area with respect to the low moisture content of the surrounding area. In this study, satellite image/ data, LANDSAT 7 is acquired for EQ affected area before and after the EQ. These images contain data of different bands information in terms of Digital Numbers (DN). The DN is first converted to Radiance. The value of the radiance is affected by the atmospheric condition of the area. So, atmospheric correction is carried out by using the FLAASH module in ENVI software. The thermal infrared spectrum of the satellite data is used for calculating the radiant temperature. With the help of Planck's radiation equation, spectral radiance is converted to the temperature. As soil surface temperature decreases with increasing soil water content, it can be correlated with soil moisture content. After finding the soil moisture content, the pre and/or post-earthquake(EQ) satellite are compared to find out the changes. On the basis of the changes and soil moisture contain difference between nearby area the probable post EQ liquefaction features positions are found out for the region.

Keywords: Liquefaction; Remote sensing; Soil moisture content.

1 INTRODUCTION

Studying satellite data or image is the way to get information about an area without going to that particular area. Thus it helps in acquiring data from a remote place. This also reduces time effort and money in finding different features, objects etc. in a particular location. As the data acquisition is done from the sky, satellite remote sensing can be used to collect data for different spectral bands with required spatial and temporal resolutions. Thus satellite image can be used to capture data before and after an event. Information obtain from various spectral bands can be used to find the properties of the earth surface. Many researchers have studied different earthquake (EQ) induced effects by comparing the pre- and post-EQ images (Gupta et al., 1995; Kohiyama and Yamazaki, 2005; Rathje et al., 2005; Huyck et al., 2006; Rathje et al., 2006; and Eguchi et al., 2010). Satellite image can be used in two ways; either both pre- and post-earthquake data can be used to identify change or the only post-EQ imagery can be used to identify the damage (Oommen et al. 2013). In this study, both pre- and post EQ data are used for identification of liquefaction features.

North East (NE) India is seismically most active region in entire India. All places of the NE India are situated in Zone V of seismic zonation of India (IS-1893, 2016). In past, many major and great EQs were occurred in the area. During those major and great EQs in many places of the region were undergo liquefaction (Rastogi et al., 1993). During 1869 Cachar EQ (7.5 Mw), liquefaction features were occurred in in Manipur, along the banks of the Jiri River and in North Cachar region Oldham1899. During 1897 Assam earthquake (8.1 Mw), large numbers of liquefaction occurred throughout the Assam valley (Oldham 1899, Baro and Kumar 2015). During 2017 Manu earthquake (5.6 Mw) which is a moderate EQ, liquefaction features were observed near the epicentral region in Tripura (Debbarma et al., 2017).

The objective of this study is to find the probable liquefaction induced surface features in NE India region occurred after an EQ, using satellite image and different bands data. As per Oommen et al. 2013, when liquefaction occurs, soil moisture increases in a particular area compare to the surrounding non-liquefied areas. These can be determined by finding the wetness of the areas on the basis of the reflectance values of different bands. The increase in soil moisture results in decrease in temperature of the area which can be found by using reflectance information of different bands such as thermal infrared (TIR) and shortwave infrared (SWIR) (Yusuf et al., 2001) of the satellite data. By comparing this information of pre and post EQ satellite data the probable liquefaction is identified in the study.

2 METHODOLOGY

In this study the method proposed by Oommen et al. 2013 is used for finding the probable liquefaction feature in an area where EQ was occurred. The soil temperatures and soil moistures difference obtain from the pre and post EQ satellite images are calculated to find whether the soil was undergoing liquefaction or not. The method is described below.

2.1 Digital Number to Radiance

On a satellite images, collected from different source the reflected energy which is captured by the sensor for different band is represented as a Digital Number (DN). This DN need to be converted to reflectance first. To do so first it is needed to convert to radiance. Radiance is the energy that the sensor detect which come from the objects (Pandya et al., 2002; Srinivasulu and Kulkarni, 2003). The DN which is dependent on the satellite sensor property can be calculated by using the calibration parameters and radiometric resolution of the satellite sensors. In this study, following relation is used to find out the Radiance from DN number value for different band (Chander et al., 2009).

$$L_\lambda = L_{min\lambda} + \frac{L_{max\lambda} - L_{min\lambda}}{Q_{cal\ max} - Q_{cal\ min}}(Q_{cal} - Q_{cal\ min})$$

Here, L_λ is the spectral radiance, $L_{min\lambda}$ and $L_{max\lambda}$ are the minimum and maximum spectral radiance values of the satellite sensor corresponding to the gain settings at the time of acquisition, $Q_{cal\ max}$ is the maximum possible DN value and $Q_{cal\ min}$ is the minimum possible DN value. For the Landsat ETM$^+$ sensors $Q_{cal\ max}$= 255 and $Q_{cal\ min} = 1.$, $L_{min\lambda}$ and $L_{max\lambda}$ for different band of Landsat ETM$^+$ satellite is given in the Table 1(Chander et al., 2009).

Table 1: Spectral Radiance Range (Watts/(m² * sr * µm)) for LANDSAT-7 bands (Chander et al., 2009)

Bands	Low Gain		High Gain		Bands	Low Gain		High Gain	
	$L_{min\lambda}$	$L_{max\lambda}$	$L_{min\lambda}$	$L_{max\lambda}$		$L_{min\lambda}$	$L_{max\lambda}$	$L_{min\lambda}$	$L_{max\lambda}$
Band1	6.2	293.7	6.2	191.6	Band5	1	47.57	1	31.06
Band2	6.4	300.9	6.4	196.5	Band6	0	17.04	3.2	12.65
Band3	5	234.4	5	152.9	Band7	0.35	16.54	0.35	10.80
Band4	5.1	241.1	5.1	157.4	Band8	4.7	243.1	4.7	158.3

2.2 Radiance to Temperature

The spectral radiance of the thermal band (band 6 of Landsat ETM^{+}) can be used to calculate the At-satellite brightness temperature. This can be done by using the following relation (Chander et al., 2009).

$$T = \frac{K_2}{\ln\left(\frac{K_1}{L_\lambda} + 1\right)}$$

Where, T is the Effective at-sensor brightness temperature in K, K_1 and K_2 are the calibration constants and L_λ is the at sensor spectral radiance in W/(m2 sr µm). For Landsat ETM$^+$ L1 data K_1= 666.09 Watts/(m² sr µm) and K_2= 1282.71 K. For this study, the land surface temperature (LST) is considered approximately equal to this at-sensor brightness temperature.

2.3 Atmospheric Correction

The data sensed by the sensor in the space contain information about both earth surface and atmosphere as the energy has to pass through the atmosphere to reach the satellite. For this to know about the earth surface properties it is required to remove the effect of the atmospheric substances. This process is called atmospheric correction. In this study, the FLAASH module of ENVI is used for atmospheric correction of the Landsat 7 data for bands 1–5 and band 7 (Adler-Golden et al., 1999; Matthew et al.,2000).

The information about scene, data acquisition time and sensor are needed for using the FLAASH. This information can be found from the METADATA file of the Landsat ETM+ data source folder. The tropical atmospheric model is selected for all the images based on the latitude of the areas. 40 km initial visibility is assumed. Output file of the FLAASH contains at-surface reflectance information of the image.

2.4 Tasseled Cap Transformation

Tasseled Cap transformation is used to convert the reflectance values of Landsat ETM+ bands to six axes. This six axes include three major axes which gives physical characteristics values like brightness, greenness, and wetness. As per Oman et al. 2013, we can use of the Landsat ETM+ image tasseled cap transform wetness axes to find the surface wetness/moisture in the pre- and post-earthquake coverage to find out the liquefaction. Huang et al. (2002) developed the tasseled cap transformation coefficients for Landsat 7 bands reflectance values. The coefficients are given in Table 2. For this study, these coefficients are used for the transformation.

Table 2: Tasseled cap coefficients for Landsat 7 at-satellite reflectance (Huang et al., 2002)

Index	Band 1	Band 2	Band 3	Band 4	Band 5	Band 7
Brightness	0.3561	0.3972	0.3904	0.6966	0.2286	0.1596
Greenness	20.3344	20.3544	20.4556	0.6966	20.0242	20.263
Wetness	0.2626	0.2141	0.0926	0.0656	20.7629	20.5388
Fourth	0.0805	20.0498	0.195	20.1327	0.5752	20.7775
Fifth	20.7252	20.0202	0.6683	0.0631	20.1494	20.0274
Sixth	0.4	20.8172	0.3832	0.0602	20.1095	0.0985

2.5 Change Detection

In this study, the change detection is performed by differencing the Post and pre EQ images:

$$D(x) = I_2(x) - I_1(x)$$

Where, D(x) is the difference image, $I_2(x)$ and $I_1(x)$ are the post-earthquake and pre-earthquake images respectively. The results of this differencing gives positive and negative values for the areas where change is there and gives near zero for the area where there is no or little change. Image standardization is applied to the images before the image differencing is carried out as per suggestion by Warner and Chen, 2001 and Oman et al. 2013.

3 STUDY AREA AND DATA COLLECTION

In January 4 2016, Manipur EQ occurred with a magnitude of 6.7 Mw. In this study, the nearby areas of the origin of the EQ is taken as study area (Figure 1). As situated in Zone V many Major EQs affect the area and in past study shows that there are many liquefactions happened in those areas. Landsat 7 images for the area are collected from the earthexplorer site (https://earthexplorer.usgs.gov/). One pre EQ image (Date 24.12.2015) and one post EQ image (date 25.01.2016) are collected for the study. For detecting the liquefaction, the area which have less vegetation and plain are considered. Standard false colour composite (FCC) of the area is shown in the Figure 2. For the study, the area covered by the green rectangle in the Figure 2 is taken as study area as it has less vegetation and no cloud coverage.

4 RESULTS AND DISCUSSION

Above methodology is followed to obtain the LST and wetness value for the both images. After this, image standardization is applied to the images in both the cases and differencing is carried out. Figure 3(a) shows the temperature difference image between the pre- and post-earthquake wetness images. Similarly, the wetness difference image is obtained from pre- and post-earthquake temperature images (Figure 3(b)). Figure 4(a) shows the areas of extreme decrease in temperature, considering change in the temperature value less than -1.5 standard deviation as the extreme decrease in LST as per Oman et al. 2013. In Figure 4(b), the areas of extreme increase in wetness is shown. In this study, a change in the wetness value more than 1.5 standard deviation is considered as the extreme increase in wetness as per Oman et al. 2013 Areas of extreme changes where there is no vegetation and no cloud coverage are considered as the areas where liquefactions were occurred during the EQ.

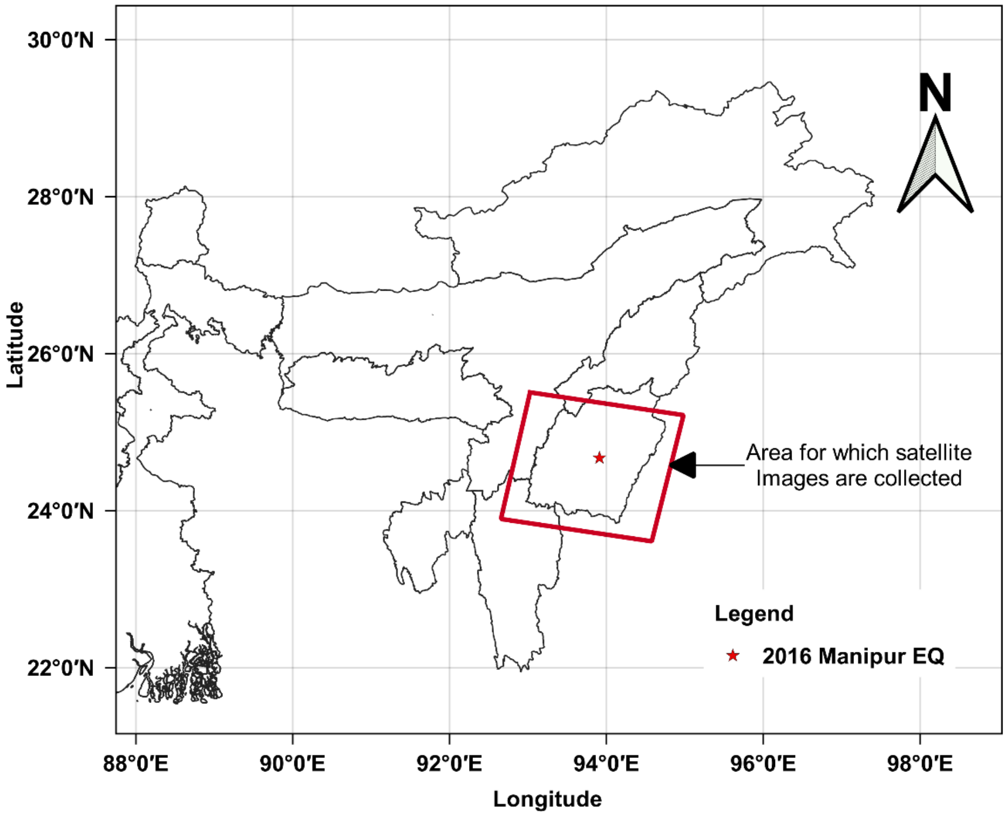

Figure 1: Figure showing the NE India and the area for which the satellite images are collected

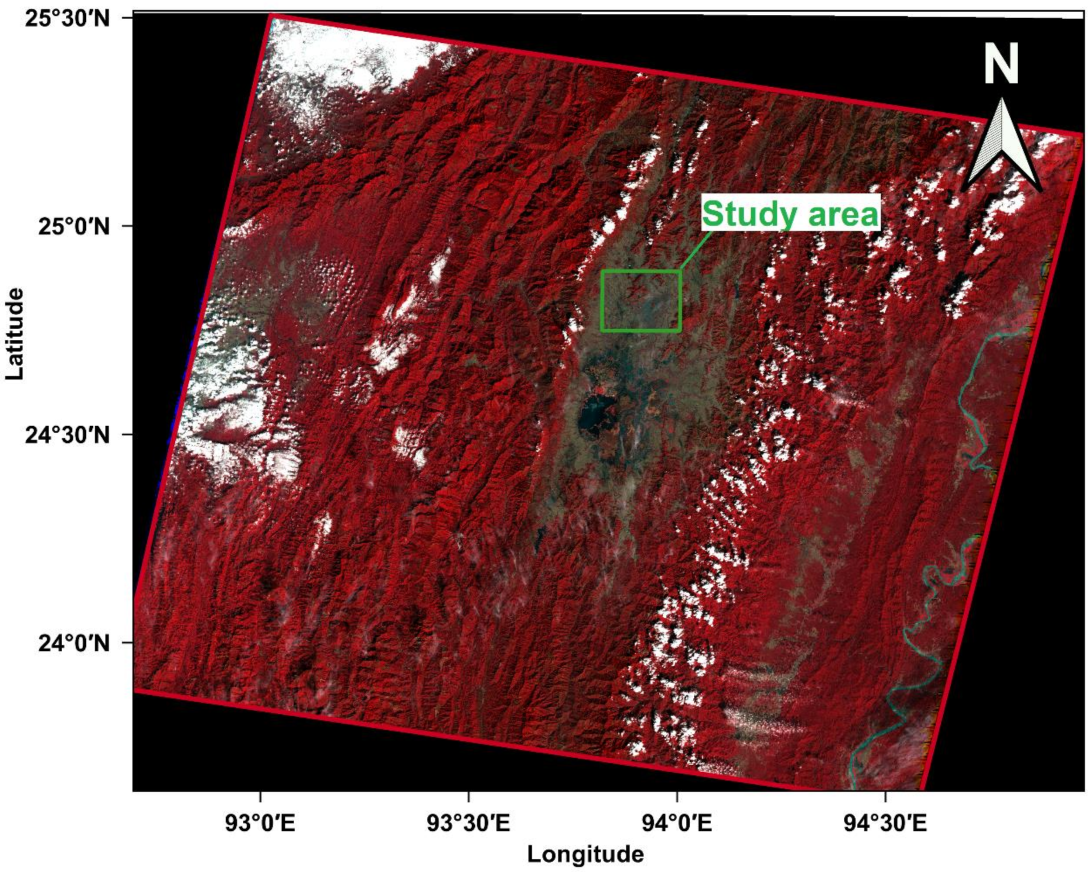

Figure 2: Standard FCC of LANDSAT 7 satellite data of the region and the study area

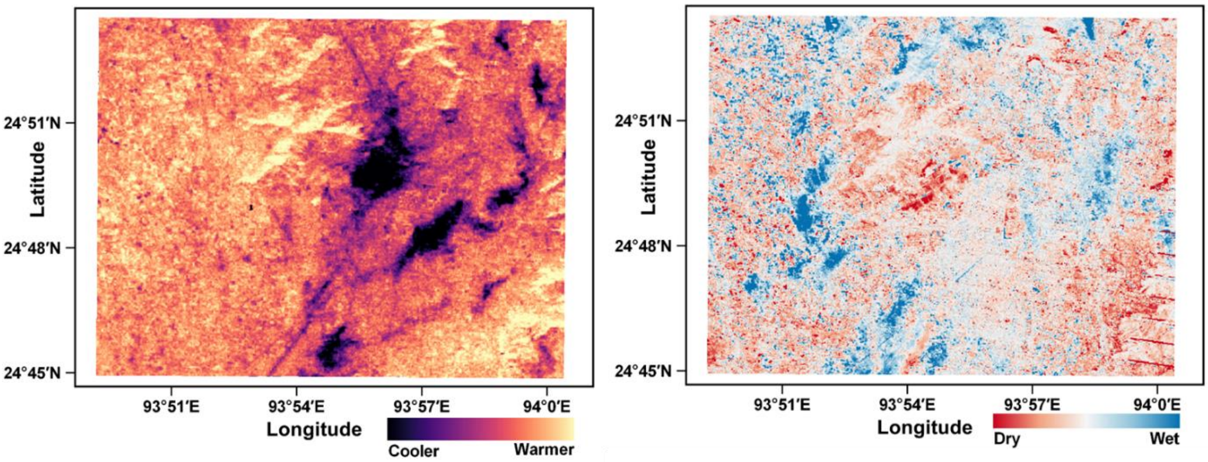

Figure 3: Pre and post EQ image difference for (a) LST, (b) Wetness

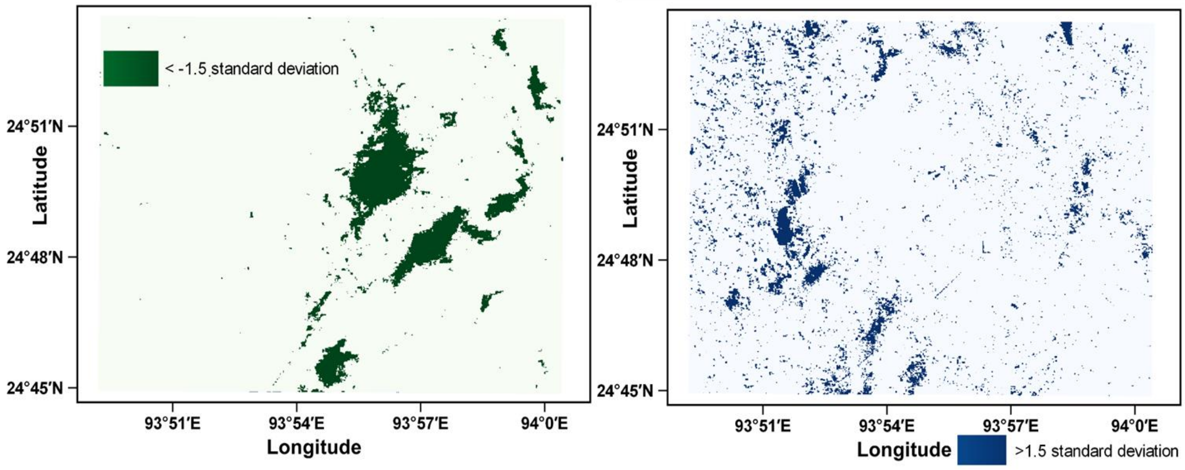

Figure 4: Images showing extreme changes (a) areas of LST changes <-1.5 standard deviation, (b) areas of wetness changes > 1.5 standard deviation

From Figure 3 (a) and (b) it can be seen that for some parts where there is increase in temperature the wetness is increase in those places also. Similarly, Figure (a) and (b) also show that those places where extreme reduction in LST the extreme increase in wetness is not occurred there. Only some places which are located East and south part in the images there is both extreme decrease in LST and extreme increase in wetness. The result of the present study does not confirm about the liquefaction occurred but gives a probable identification of the liquefaction. The result of the study will help to carry out field investigation in the area for finding liquefaction in future.

5 CONCLUSIONS

From the above study, it is found that there are many places where liquefaction might be occurred during the 2016 Manipur EQ. As most of the NE India region is hilly and covered with vegetation finding liquefaction features by using satellite image is difficult. For the study, area which have plain topography and less vegetation is considered. Due to the presence of the cloud, satellite image just after 5 days of the EQ is not taken for the study. That can give a better result. For the study, LST taken as equal to at sensor brightness temperature. In future, estimated LST may be used for the detection of area undergo liquefaction.

REFERENCES

[1] Adler-Golden, S. M., Matthew, M. W., Bernstein, L. S., Levine, R. Y., Berk, A., Richtsmeier, S. C., Acharya, P. K., Anderson, G. P., Felde, G. W., Gardner, J., Hoke, M. P., Jeong, L. S., Pukall, B., Mello, J., Ratkowski, A., And Burke, H. H. (1999). Atmospheric Correction for Short-Wave Spectral Imagery Based on MODTRAN4. *Society of Photooptical Instrumentation*

Engineers (SPIE) Proceeding, Imaging Spectrometry, 3753, 61–69

[2] Baro O and Kumar A. 2015. A review on the tectonic setting and seismic activity of the Shillong plateau in the light of past studies. *Disaster Advances*, 8(7), 34–45

[3] Chander, G.; Markham, B.; and Helder, D. (2009). Summary of current radiometric calibration coefficients for Landsat MSS, TM, ETM+, and EO-1 ALI sensors. *Remote Sensing of Environment*, 113(5), 893–903.

[4] Debbarma, J., Martin, S.S., Suresh, G., Ahsan, A. and Gahalaut, V.K. (2017). Preliminary observations from 3 January 2017 MW 5.6 Manu, Tripura (India) earthquake, *Journal of Asian Earth Sciences*, doi: http://dx.doi.org/10.1016/j.jseaes.2017.08.030

[5] Eguchi, R. T.; Gill, S. P.; Ghosh, S.; Svekla, W.; Adams, B. J.; Evans, G.; Toro, J.; Saito, K.; And Spence, R. 2010). The January 12, 2010, Haiti earthquake: A comprehensive damage assessment using very high resolution areal imagery. *In 8th International Workshop on Remote Sensing for Disaster Management*, Tokyo Institute of Technology, Tokyo, Japan.

[6] Gupta, R. P.; Chander, R.; Tewari, A. K.; And Saraf, A. K. (1995). Remote-sensing delineation of zones susceptible to seismically induced liquefaction in the Ganga plains. *Journal of the Geological Society of India*, 46(1), 75–82.

[7] Huang, C.; Wylie, B.; Yang, L.; Homer, C.; And Zylstra, G. (2002). Derivation of a tasselled cap transformation based on Landsat 7 at satellite reflectance. *International Journal of Remote Sensing*, 23(8),1741–1748.

[8] Huyck, C.; Matsuoka, M.; Takahashi, Y.; And Vu, T. (2006). Reconnaissance technologies used after the 2004 Niigata-ken Chuetsu, Japan, earthquake. *Earthquake Spectra*, 22, 133–145.

[9] IS:1893 part1 (2016). Criteria for Earthquake Resistant Design of Structures, Bureau of Indian Standards, New Delhi, India

[10] Kohiyama, M. And Yamazaki, F. (2005). Damage detection for 2003 Bam, Iran, earthquake using Terra-Aster satellite imagery. *Earthquake Spectra*, 21(S1), 267–274.

[11] Matthew, M. W.; Adler-Golden, S. M.; Berk, A.; Richtsmeier, S. C.; Levine, R. Y.; Bernstein, L. S.; Acharya, P. K.; Anderson, G. P.; Felde, G. W.; Hoke, M. P.; Ratkowski, A., Burke, H. H.; Kaiser, R. D.; And Miller, D. P. (2000). Status of atmospheric correction using a MODTRAN4-bashed algorithm. *Society of Photo-optical Instrumentation Engineers (SPIE) Proceeding, Algorithms for Multispectral, Hyperspectral, and Ultraspectral Imagery*, 4049, 199–207

[12] Oldham R.D. (1899)Report on the Great Earthquake of 12 June 1897, *Memoir Geol.Surv. India*,29, 379

[13] Pandya, M. R.; Singh, R.; Murali, K. R.; Babu, P. N.; Kirankumar, A. S.; And Dadhwal, V. K. (2002). Bandpass solar exoatmospheric irradiance and Rayleigh optical thickness of sensors on board Indian remote sensing satellites-1B, -1C, -1D, and P4. *IEEE Transactions on Geoscience and Remote Sensing*, 40(3, pp), 714–718

[14] Rastogi B.K., Chadha R.K., and Rajgopalan G. (1993) Paleoseismicity studies in Meghalaya, *Curr. Sci*., 64(11&12), 933- 935

[15] Rathje, E.; Kayen, R.; And Woo, K. S. (2006). Remote sensing observations of landslides and ground deformation from the 2004 Niigata Ken Chuetsu earthquake. *Soils and Foundations*, 46(6), 831–842

[16] Srinivasulu, J. And Kulkarni, A. V. (2003). Estimation of spectral reflectance of snow from IRS-1D LISS-iii sensor over the Himalayan terrain. *Journal of Earth System Science*, 113(1), 117–128.

[17] Warner, T. A. And Chen, X. (2001). Normalization of Landsat thermal imagery for the effects of solar heating and topography. *International Journal of Remote Sensing*, 22(5), 773–788

[18] Yusuf, Y.; Matsuoka, M.; And Yamazaki, F. (2001). Damage assessment after 2001 Gujarat earthquake using Landsat-7 satellite images. *Journal of the Indian Society of Remote Sensing*, 29(1), 3–16.